Ground-state phase diagram of the two-dimensional extended Bose-Hubbard model

Takahiro Ohgoe,[1,*] Takafumi Suzuki,[2] and Naoki Kawashima[1]

[1]*Institute for Solid State Physics, University of Tokyo, Kashiwa, Chiba 277-8581, Japan*

[2]*Research Center for Nano-Micro Structure Science and Engineering, Graduate School of Engineering, University of Hyogo, Himeji, Hyogo 671-2280, Japan*

(Received 2 July 2012; published 27 August 2012)

We investigate the ground-state phase diagram of the soft-core Bose-Hubbard model with the nearest-neighbor repulsion on a square lattice by using an unbiased quantum Monte Carlo method. In contrast to a previous study [P. Sengupta *et al*., Phys. Rev. Lett. **94**, 207202 (2005)], we present the ground-state phase diagrams up to high hopping amplitudes. As a result, in addition to the known supersolid above half-filling, we find a supersolid phase below and at half-filling for high hopping amplitudes. In addition, for a strong nearest-neighbor repulsion, we show that the supersolid phase occupies a remarkably broad region in the phase diagram. These results are in agreement with the results of the Gutzwiller mean-field approximation [M. Iskin, Phys. Rev. A **83**, 051606(R) (2011); T. Kimura, Phys. Rev. A **84**, 063630 (2011)]. However, it turns out that the regions of the supersolid phases are significantly smaller than the mean-field results.

DOI: 10.1103/PhysRevB.86.054520 PACS number(s): 03.75.Hh, 05.30.Jp, 67.85.−d

I. INTRODUCTION

Supersolids (SSs) have attracted great interest for a long time as a fascinating quantum state that has superfluidity and solidity simultaneously. In the early theoretical works by Andreev and Lifshitz[1] and Chester,[2] they proposed a scenario in which a SS might appear when zero-point defects in a solid such as ^{4}He undergo Bose-Einstein condensation at low temperatures without destroying the crystal structure. Several decades later, a discovery was made in 2004 by Kim and Chan.[3,4] In their experiments on solid ^{4}He, they observed nonclassical rotational inertia associated with superfluidity in the solid. After this discovery, further theoretical and experimental works[5–7] provided evidence that the SS-like behavior in solid ^{4}He is different from that of a bulk SS based on the Andreev-Lifshitz-Chester scenario. The superfluidity in solid ^{4}He seems to appear as a result of the extended defects such as grain boundaries[8,9] and dislocations.[10]

In contrast to continuous spaces, lattice systems have recently been considered to be promising candidates for realizing an SS. This is due to the recent experimental development of optical lattice systems.[11–14] Ultracold Bose gases trapped in optical lattices are ideal systems for realizing the Bose-Hubbard models.[15] As a result of intensive theoretical and numerical studies, the existence of SS phases has been established in extended Bose-Hubbard models.[16–31] Most of the SSs in lattice systems are achieved by doping particles or holes into insulating solid states at commensurate filling factors. If doped defects delocalize and undergo Bose-Einstein condensation rather than a phase separation, a SS appears in accordance with the Andreev-Lifshitz-Chester scenario. Thus, the resulting SSs are stabilized at incommensurate filling factors.

One of the simplest models used to study SSs is the soft-core Bose-Hubbard model with nearest-neighbor repulsion. By performing accurate quantum Monte Carlo calculations on this model, a checkerboard (CB) SS phase has been found on a one-dimensional (1D) chain,[22] a 2D square lattice,[21] and a 3D simple cubic lattice.[26,30,32] In the 1D and 2D cases, the SS phase is found only above half-filling (interstitial SSs). In contrast, in the 3D case, the SS phase is found not only above half-filling but also below and at half-filling for high hopping amplitudes (vacancy SSs and commensurate SSs, respectively).[26,30,32] In particular, the presence of an SS at a commensurate filling factor of $1/2$ is fascinating as an exceptional SS *without any doping*, although it has not yet been found in lower dimensions. Therefore, it is an open question why there is a discrepancy in the results in the 2D versus 3D systems.

Recent works based on the Gutzwiller mean-field approximation have provided some interesting results on the ground-state phase diagram of the extended Bose-Hubbard model,[33,34] including a possible answer to the above question. In the ground-state phase diagram presented in Ref. 33, the author found a SS phase below and at half-filling. Since the SS phase is clearer for higher hopping amplitudes, he suggested that the absence of such a SS region in the 2D quantum Monte Carlo study[21] might be due to the low hopping amplitude. However, the SS phase below and at half-filling is much smaller than that above half-filling. In addition, the validity of the Gutzwiller mean-field approximation is not clear for the region around half-filling in the 2D system, although it becomes more accurate when the dimensionality and the particle density increases. Thus, to conclude the existence of a 2D SS phase below and at half-filling, more precise treatments are desirable.[33]

The other interesting result presented in Ref. 34 is on SS phases for a strong nearest-neighbor repulsion. The ground-state phase diagrams show that as the nearest-neighbor repulsion increases, the SS phase expands up to high hopping amplitudes in the phase diagram. In particular, the 2D case of this result is important, because it could be realized in quasi-2D dipolar Bose gases whose dipoles are polarized along the z axis.[35] Therefore, from an experimental viewpoint, we should also determine more precise phase boundaries in the 2D system and verify the accuracy of the phase diagram.

In this paper, motivated by the results of the Gutzwiller approximation, we investigate the ground-state phase diagram of the extended Bose-Hubbard model on a square lattice by numerically exact quantum Monte Carlo simulations.

The paper is organized as follows. In Sec. II, we describe the model discussed in this paper and the quantum Monte Carlo method we used. Section III presents the ground-state phase diagrams in the grand-canonical ensemble. These phase diagrams include insulating lobes up to the third lobe. Within this region, we confirm that our ground-state phase diagrams are in qualitative agreement with those obtained by the Gutzwiller approximation. In Sec. IV, we study quantum phase transitions and explain the procedure used to determine the phase boundaries presented in the previous section. In Sec. V, we investigate the SS phase at half-filling by obtaining results for the canonical ensembles. By constructing a ground-state phase diagram at half-filling, we confirm that the SS phase is easily found for high hopping amplitudes. Finally, in Sec. VI, we summarize our results.

II. MODEL AND METHOD

The model considered in this paper is the soft-core Bose-Hubbard model with nearest-neighbor repulsion on a square lattice. The Hamiltonian is given by

$$H = -t\sum_{\langle i,j\rangle}(b_i^\dagger b_j + \text{H.c.}) - \mu\sum_i n_i + \frac{U}{2}\sum_i n_i(n_i-1) + V\sum_{\langle i,j\rangle} n_i n_j. \quad (1)$$

Here, $b_i^\dagger(b_i)$ is the bosonic creation (annihilation) operator on site i, and n_i is the particle number operator defined by $n_i = b_i^\dagger b_i$. The summation $\langle i,j\rangle$ is taken over all pairs of nearest-neighbor sites. For a square lattice, the coordination number z is 4. Furthermore, t is the hopping amplitude, μ is the chemical potential, U is the on-site interaction, and V is the nearest-neighbor interaction. In this paper, we consider the case where the interactions are repulsive ($U,V > 0$). In our simulations, we treat systems of the size $N = L \times L$ with the periodic boundary condition.

In the classical limit $t/U = 0$, the ground states are known and simple.[21,30,34] When the nearest-neighbor repulsion satisfies $zV/U < 1$, the ground states are CB solids at filling factors $\rho = 1/2,\ 3/2,\ldots$ and uniform Mott insulators at $\rho = 1,2,\ldots$. To characterize each state, we can label it (n_A,n_B), which represents a pair of particle numbers on the two sublattices A and B. Without loss of generality, we assume that $n_A \geqslant n_B$. On the basis of this notation, the ground states are labeled (1,0), (1,1), (2,1), (2,2),... at $\rho = 1/2,\ 1,\ 3/2,\ 2,\ldots$, respectively. In contrast, for $zV/U > 1$, all ground states are CB solids. The states are labeled (1,0), (2,0), (3,0), (4,0),... at $\rho = 1/2,\ 1,\ 3/2,\ 2,\ldots$, respectively, and the transition from $\rho = n/2$ to $(n+1)/2$ takes place at $(\mu/U)_c = n$ when the chemical potential is increased. Therefore, $zV/U = 1$ is a critical point for $\rho \geqslant 1$ in the classical limit. When a finite t/U is introduced, the critical point $(zV/U)_c = 1$ is shifted to a slightly larger value due to quantum fluctuations.

To investigate the properties of the model for finite values of t/U, we used an unbiased quantum Monte Carlo method. The formulation we used is based on the Feynman path integral representation. In the representation, the d-dimensional quantum system is mapped to $(d+1)$–dimensional classical systems. In the mapped systems, each configuration is considered as a world line with d-dimensional space axes and a 1D imaginary time axis. On the basis of this representation, we sample the world-line configurations using the Markov chain Monte Carlo method. To update the configurations, we used a worm-type algorithm.[36–39]

III. GROUND-STATE PHASE DIAGRAMS IN THE GRAND-CANONICAL ENSEMBLE

In this section, we present ground-state phase diagrams in the zt/U-μ/U plane. A recent Gutzwiller mean-field study suggested that the SS phase might exist below half-filling for high hopping amplitudes.[33] In addition, another work showed that the ground-state phase diagram has qualitatively different structures between weak and strong nearest-neighbor repulsions.[34] Remarkably, in the latter case, the SS phase seems to occupy a very large region in the phase diagram. To confirm these results by numerically exact quantum Monte Carlo calculations, we show the ground-state phase diagrams at $zV/U = 1$ and $zV/U = 1.5$ in Secs. III A and III B, respectively.

A. Ground-state phase diagram at $zV/U = 1$

In Fig. 1(a), we show the ground-state phase diagram at $zV/U = 1$ in the zt/U-μ/U plane. To detect each phase, we measured the particle density $\rho = 1/N\sum_i\langle n_i\rangle$, the superfluid (SF) stiffness $\rho_s = \langle \boldsymbol{W}^2\rangle/(2dt\beta L^{d-2})$, and the structure factor $S(\boldsymbol{k}) = 1/N^2\sum_{i,j} e^{i\boldsymbol{k}\cdot\boldsymbol{r}_{ij}}(\langle n_i n_j\rangle - \langle n_i\rangle^2)$. Here, $\langle\cdots\rangle$ is the thermal average and $\boldsymbol{W}$ denotes the winding number vector

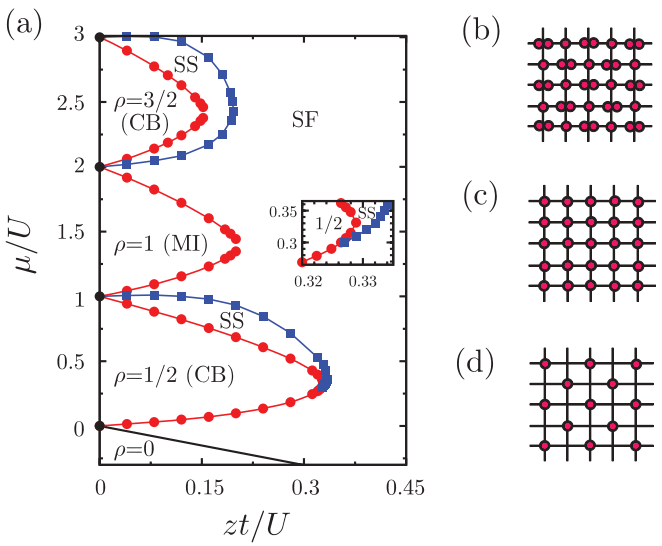

FIG. 1. (Color online) (a) Ground-state phase diagram of the extended Bose-Hubbard model on a square lattice at $zV/U = 1$. The (red) circles indicate boundaries of the insulating lobes; (blue) squares represent the SS-SF boundary. Inset: Enlarged view of the region around the tip of the first CB lobe. Error bars are drawn but most of them are much smaller than the symbol size (here and in the following figures). The solid (black) line is the boundary between the empty region and the SF, which can be obtained analytically. Other lines are guides for the eyes. (b–d) Schematic configurations of the insulators at (b) $\rho = 3/2$, (c) $\rho = 1$, and (d) $\rho = 1/2$. Each filled (red) circle represents one particle at a site.

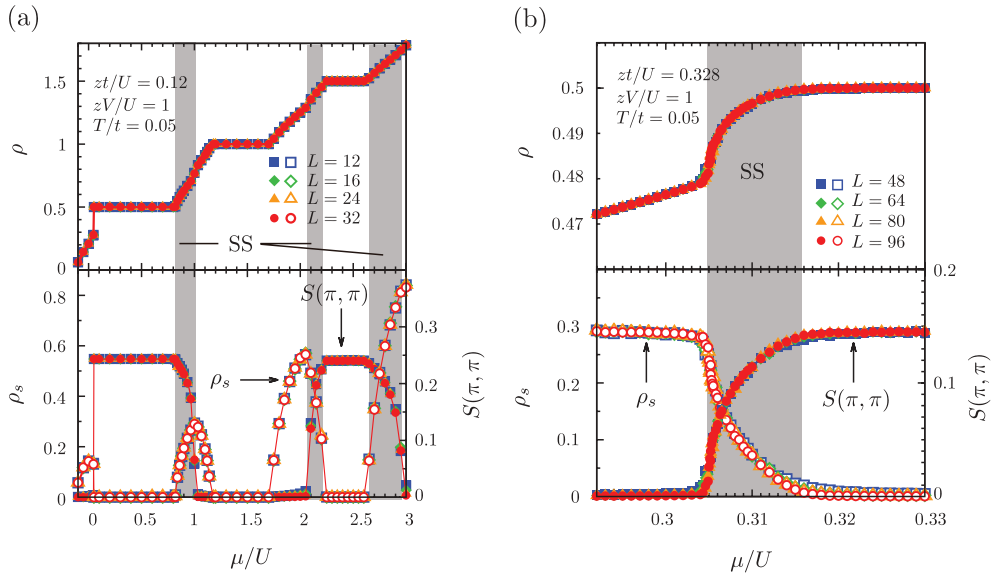

FIG. 2. (Color online) Particle density ρ, superfluid stiffness ρ_s, and structure factor $S(\pi,\pi)$ as functions of the chemical potential μ/U at (a) $(zt/U,zV/U,T/t) = (0.12,1,0.05)$ and (b) $(zt/U,zV/U,T/t) = (0.328,1,0.05)$. Shaded regions indicate the supersolid state where ρ_s and $S(\pi,\pi)$ take finite values simultaneously.

in the path integral representation.[40] β represents the inverse temperature defined by $\beta = 1/T$, d is the dimensionality of the system, which is 2 in this paper, $\boldsymbol{k}$ is the wave vector, and $\boldsymbol{r}_{ij}$ is the relative position vector between site i and site j. In our phase diagram up to $\mu/U = 3$, in addition to a conventional SF phase, there are three insulating lobes, at $\rho = 1/2$, $\rho = 1$, and $\rho = 3/2$, whose schematic configurations are shown in Figs. 1(b), 1(c), and 1(d), respectively. The lobe at $\rho = 1$ is a uniform Mott insulating (MI) phase, and the others at $\rho = 1/2$ and $\rho = 3/2$ are CB solid phases characterized by a finite value of $S(\pi,\pi)$. We also confirm the presence of SS phases around the insulating CB lobes. The determination of the phase boundaries is explained in detail in Sec. IV.

To show the existence of each phase, we plot the μ/U dependence of the measured quantities at $(zt/U,zV/U,T/t) = (0.12,1,0.05)$ and (0.328, 1, 0.05) in Figs. 2(a) and 2(b), respectively. In the case of the low hopping amplitude $zt/U = 0.12$ in Fig. 2(a), SS phases exist above $\rho = 1/2$ and around $\rho = 3/2$. When particles are removed from the CB solid at $\rho = 1/2$, the possible SS is unstable against phase separation, as known by the strong-coupling argument.[21] In contrast, for the higher hopping amplitude $zt/U = 0.328$ in Fig. 2(b), we find that the SS phase is present even below half-filling. As shown in the inset in Fig. 1(a), the SS phase covers the tip of the first CB lobe. This result suggests that the SS can also be stabilized at half-filling. In Sec. V, we present direct evidence for the SS at half-filling by obtaining results for the canonical ensemble and excluding possible phase separations. In addition to the SS around $\rho = 1/2$, the other SS phase around $\rho = 3/2$ more clearly covers the tip of the corresponding insulating CB lobe. Therefore, the SS seems to be stabilized even at $\rho = 3/2$. The present 2D ground-state phase diagram is in agreement with that in the 3D system[32] and the results of the Gutzwiller mean-field approximation.[16,34,41] However, we have found that the SS regions clearly become smaller as the dimensionality decreases.

B. Ground-state phase diagram at $zV/U = 1.5$

For strong nearest-neighbor repulsions, all insulating states are CB solid states and, thus, the ground-state phase diagram is quite different from that for weak nearest-neighbor repulsions. In Fig. 3(a), we present the ground-state phase diagram at $zV/U = 1.5$ in the grand-canonical ensemble. In contrast to the phase diagram at $zV/U = 1$, all three insulating Mott lobes are CB lobes. The schematic configurations at $\rho = 3/2$, 1, and 1/2 are shown in Figs. 3(b), 3(c), and 3(d), respectively. Compared with the case of $zV/U = 1$, the insulating lobes extend up to higher hopping amplitudes. This result is reasonable, because the strong nearest-neighbor repulsion favors the CB solid state. The noteworthy point here

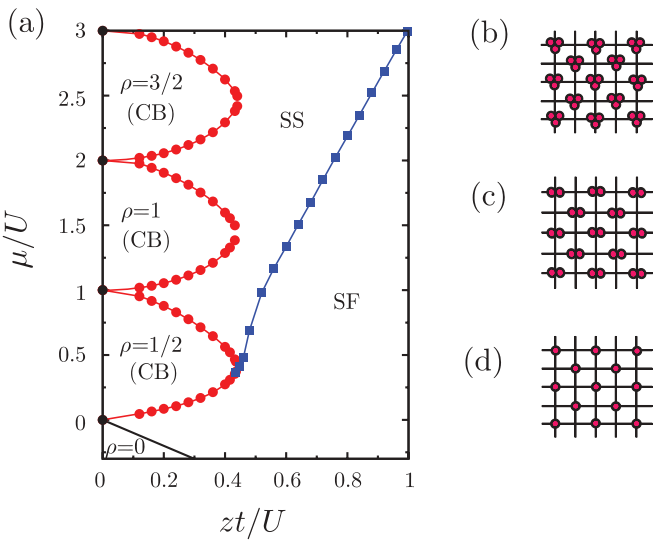

FIG. 3. (Color online) (a) Ground-state phase diagram in the zt/U-μ/U plane at $zV/U = 1.5$. (b-d) Schematic configurations of the insulators at (b) $\rho = 3/2$, (c) $\rho = 1$, and (d) $\rho = 1/2$.

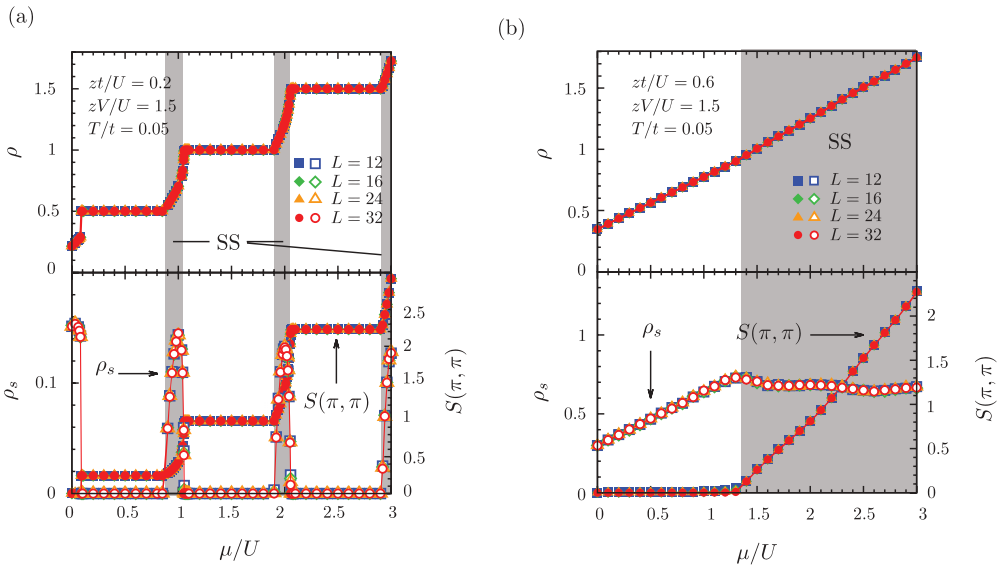

FIG. 4. (Color online) Particle density ρ, superfluid stiffness ρ_s, and structure factor $S(\pi,\pi)$ as functions of the chemical potential μ/U at (a) $(zt/U,zV/U,T/t) = (0.2,1.5,0.05)$ and (b) $(zt/U,zV/U,T/t) = (0.6,1.5,0.05)$.

is that a connected SS phase exists, which surrounds all the CB lobes. The SS phase occupies a broad region up to high hopping amplitudes, and the phase boundary behaves linearly. The presence of such a SS region is also in agreement with the results of the Gutzwiller approximation,[34] although the SS region is clearly smaller.

To verify the results, we plot the measured quantities as functions of μ/U at $(zt/U,zV/U,T/t) = (0.2,1.5,0.05)$ and (0.6, 1.5, 0.05) in Figs. 4(a) and 4(b), respectively. In Fig. 4(a), there are three plateaus, at $\rho = 1/2,1$, and $3/2$, where $S(\pi,\pi)$ takes a finite value. These plateaus correspond to the CB phases. Between these regions, $S(\pi,\pi)$ and ρ_s take finite values simultaneously, indicating the SS phase. In contrast, just below $\rho = 1/2$, there is no SS phase and we again observed a clear discontinuity in the particle density. Just below $\rho = 1$ and $3/2$, the slopes of the particle density are very steep. However, compared with those below $\rho = 1/2$, possible discontinuities are less clear. Thus, the CB-SS transitions might be weak first-order or second-order at this parameter. When the hopping amplitude decreases, we confirmed that the slopes become steeper, suggesting the presence of a first-order transition predicted by the strong-coupling argument.[21] For higher hopping amplitudes, all the insulating plateaus disappear, as shown in Fig. 4(b). In contrast, the SS phases are connected and occupy the entire regions for large chemical potentials.

Finally, we show a characteristic behavior of the correlation functions and the momentum distribution of the SS state. In Fig. 5(a), we plot the off-diagonal SF correlation function $C_{\mathrm{SF}}(\boldsymbol{r}_{ij})$ and diagonal (charge density wave) correlation function $C_{\mathrm{CDW}}(\boldsymbol{r}_{ij})$ as functions of the x coordinate at a finite temperature. The off-diagonal and diagonal correlation functions are defined by $C_{\mathrm{SF}}(\boldsymbol{r}_{ij}) = \langle b_i^\dagger b_j \rangle$ and $C_{\mathrm{CDW}}(\boldsymbol{r}_{ij}) = \langle n_i n_j \rangle - \langle n_i \rangle^2$, respectively. As shown in the lower panel in Fig. 5(a), the diagonal correlation function $C_{\mathrm{CDW}}(\boldsymbol{r}_{ij})$ shows a true long-range order. In particular, it is strongly oscillating, which indicates a strong CB order due to the large nearest-neighbor repulsion. In contrast, in the 2D system at finite temperatures, the off-diagonal correlation function $C_{\mathrm{SF}}(\boldsymbol{r}_{ij})$ shows asymptotic power-law decay, which is characteristic of the quasi-long-range order. However, the behavior is different from the conventional behavior: we can observe strongly oscillating power-law decay. This behavior is clearly due to the strong CB background potential for the SF component.[42] In Fig. 5(b), we show the resulting momentum distribution $n(\boldsymbol{k})$, which can be obtained from the Fourier transformation by $n(\boldsymbol{k}) = 1/N \sum_{i,j} C_{\mathrm{SF}}(\boldsymbol{r}_{ij}) e^{i\boldsymbol{k}\cdot\boldsymbol{r}_{ij}}$. It has a bimodal structure, with two peaks at $\boldsymbol{k} = (0,0)$ and (π,π), indicating superfluidity and CB solidity, respectively.

IV. QUANTUM PHASE TRANSITIONS

In this section, we study quantum phase transitions and explain how the phase boundaries are determined. There are three different types of quantum phase transitions in terms of symmetry breaking: the transition between two phases with different broken symmetries (CB-SF transition), transitions that involve gauge symmetry (CB-SS and MI-SF transitions), and the transition where the translational symmetry is broken (SS-SF transition). Since these quantum phase transitions have different properties related to the broken symmetries, different treatments are required to determine the phase boundaries. In the following three subsections, we explain the treatment for each phase boundary.

A. Solid-superfluid transition

We begin with the CB-SF transition, which appears at the lower boundary of the first CB lobe. As shown in Figs. 2(a) and 4(a) as well as in previous quantum Monte Carlo works,[21,30] there are finite jumps in the particle density at the boundary, indicating a first-order transition. This result can be understood from an argument based on the broken symmetries in each phase and the standard Landau-Ginzburg-Wilson paradigm. In the CB phase, the broken symmetry is the Z_2 symmetry associated with the broken translational

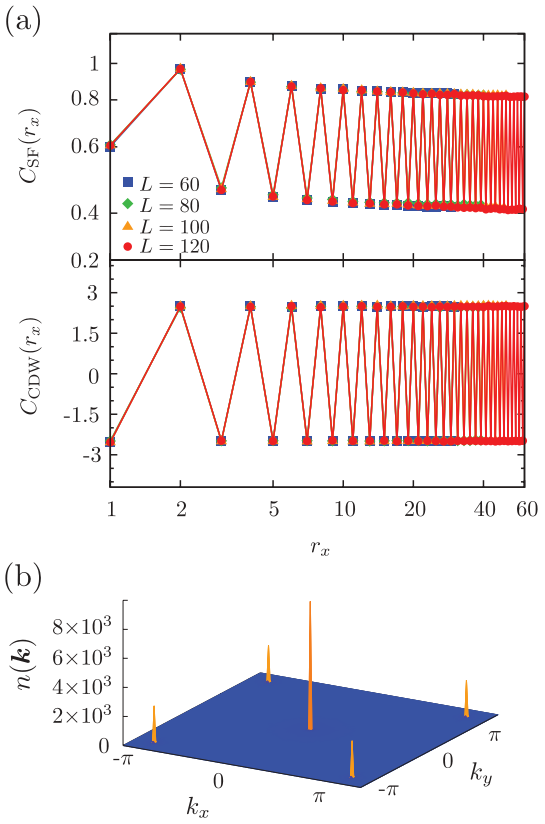

FIG. 5. (Color online) (a) Off-diagonal correlation function $C_{\rm SF}(\boldsymbol{r}_{ij})$ (upper panel) and correlation function $C_{\rm CDW}(\boldsymbol{r}_{ij})$ (lower panel) as functions of the x coordinate r_x. $C_{\rm SF(CDW)}(r_x)$ is an abbreviation for $C_{\rm SF(CDW)}(r_x,0)$. The off-diagonal correlation function is plotted on a log-log scale. The lattice spacing is set to unity. The parameter set is $(zt/U, zV/U, \mu/U, T/t) = (0.52, 1.5, 3, 0.2)$. (b) Momentum distribution near the first Brillouin zone at $L = 120$. Model parameters are the same as in (a).

symmetry. On the other hand, in the SF phase, the $U(1)$ gauge symmetry is broken *at zero temperature*. (Note that at finite temperatures in the 2D system, the SF phase shows not the long-range order but the quasi-long-range order.) According to the Landau-Ginzburg-Wilson paradigm, a transition between two phases with different broken symmetries results in a first-order transition or an intermediate region where both symmetries are broken simultaneously. Since an intermediate SS phase is absent at the boundary, the direct CB-SF transition should be first-order. Thus, we simply determined the phase boundary from the position of the finite jump in the particle density.

B. Solid-supersolid and Mott insulator–superfluid transitions

At the CB-SS boundaries and MI-SF boundaries, the quantum phase transitions are insulator-SF transitions. For the value of the dynamical critical exponent z_c, two possibilities are expected: a generic transition with $z_c = 2$ and a special transition with $z_c = 1$.[43] Because of this difference, we have to determine the transition points in different manners.

Generic transitions are driven by adding/removing a particle to/from insulating phases. In this case, the phase boundary can be determined by the finite-size scaling analysis of ρ_s for

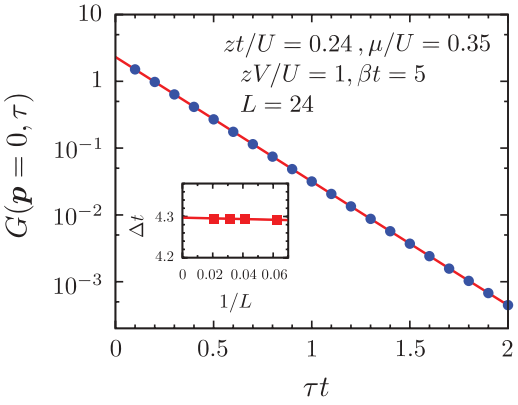

FIG. 6. (Color online) Extraction of the energy gap $\Delta_{(+)}$ from the zero-momentum Green function $G(\boldsymbol{p} = 0, \tau)$ in the first CB lobe. Filled circles denote the results obtained by our simulation, and the line represents the exponential fit. Inset: Extrapolation of the obtained Δ [(red) squares] to the thermodynamic limit.

quantum critical points with $z_c = 2$.[44] However, it can also be determined more simply from the zero-momentum Green function $G(\boldsymbol{p} = 0, \tau)$.[45,46] In the worm algorithm, the zero-momentum Green function can be obtained by measuring the Matsubara Green function $G(\boldsymbol{r}_i, \tau) = \langle T_\tau b_i(\tau) b_0^\dagger(0) \rangle$. Here, T_τ indicates the time-ordering operator on the imaginary time τ, and $b_i(\tau)$ is defined by $b_i(\tau) = e^{\tau H} b_i e^{-\tau H}$. From the asymptotic exponential decay $G(\boldsymbol{p} = 0, \tau) \sim e^{-\Delta_+ \tau}$ $(\tau \gg 0)$ $[e^{\Delta_- \tau}$ $(\tau \ll 0)]$, we can estimate the energy gap Δ_+ (Δ_-) required to create single-particle (hole) excitation with the zero momentum $\boldsymbol{p} = 0$ in the insulating phases. In the grand-canonical ensemble, the energy gap corresponds to the distance between the observed point and the phase boundary in the μ direction. Thus, we determined the phase boundary from the energy gap. Figure 6 shows an example of estimating the energy gap Δ_+ in the first CB lobe.

In contrast to the generic transition, the special transition is driven by the delocalization of quantum fluctuations. This transition occurs at the tip of insulating lobes with fixed μ/U. The tip corresponds to a multicritical point where $z_c = 1$ due to particle-hole symmetry.[43] Therefore, to determine the critical point close to the tip in the inset in Fig. 1, we performed a finite-size scaling analysis of ρ_s for quantum phase transitions with $z_c = 1$. In this analysis, the scaling form is given by $\rho_s L^{d+z_c-2} = f(\delta L^{1/\nu}, \beta/L^{z_c})$, where ν is the critical exponent of the correlation length, δ denotes the distance from the critical point as $\delta = zt/U - (zt/U)_c$, and f is a scaling function. In the present case of $d = 2$ and $z_c = 1$, the value of $d + z_c - 2$ equals 1. Therefore, the curves of $\rho_s L$ for different system sizes with fixed β/L should cross at the critical point and we can simply estimate it from the crossing point. Figure 7(a) shows one example of this estimation. In this figure, we estimated the critical point as $(zt/U)_c = 0.32888(8)$ for $\mu/U = 0.331$, which is very close to the tip.

To clarify the universality class of the special transition, we next performed the finite-size scaling analysis of $\rho_s L$. In the case of $z_c = 1$, the effective dimension becomes $d + z_c = 3$. Since the symmetry broken in this transition is related to the global U(1) symmetry, this quantum phase transition is expected to belong to the 3D *XY* universality class. Using the

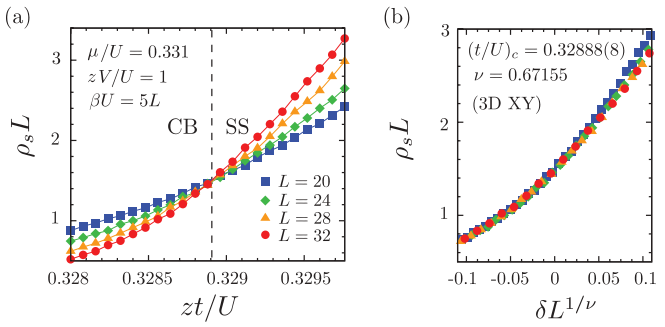

FIG. 7. (Color online) (a) Plots of $\rho_s L$ as a function of hopping amplitude zt/U near the tip of the first CB lobe. The dashed vertical line is placed at the quantum critical point $(zt/U)_c = 0.32888(8)$, which is estimated from the crossing point of the curves. (b) Scaling plots of $\rho_s L$.

critical exponent $\nu = 0.67155$ of the 3D XY universality class[47] and the dynamical critical exponent $z_c = 1$, we plot $\rho_s L$ as a function of $\delta L^{1/\nu}$ in Fig. 7(b). In this figure, we successfully observe the data collapse for large systems, supporting the validity of the present analysis.

C. Supersolid-superfluid transition

Finally, we explain the SS-SF boundaries. The SS-SF transition is the transition related to the Z_2 symmetry breaking of the translational symmetry. For this quantum phase transition, the critical point can be determined from the Binder ratio g defined by $g = 1/2[3 - \langle m^4\rangle/\langle m^2\rangle^2]$. Here, m indicates the order parameter defined by $m = 1/N \sum_i n_i e^{i\boldsymbol{k}\cdot\boldsymbol{r}_i}$ with $\boldsymbol{k} = (\pi,\pi)$. The scaling form for g is given by $g = f(\delta L^{1/\nu}, \beta/L^{z_c})$, where $\delta = zt/U - (zt/U)_c$ or $\mu/U - (\mu/U)_c$. Therefore, the curves of g for different system sizes should cross at the critical point. As a working hypothesis, we assume that the dynamical exponent z_c equals 1. In Fig. 8(a), we show the μ/U dependence of g at $zt/U = 0.24$ and $\beta t = 0.5L$. As shown in the figure, the curves cross at the same point. From the crossing point, we estimated the quantum critical point as $(\mu/U)_c = 0.08455(5)$ for $(zt/U, zV/U) = (0.24, 1)$.

To check the consistency of our analysis and clarify the universality class, we analyzed the scaling behaviors of $S(\pi,\pi)$ as well as g. The scaling form for $S(\pi,\pi)$ is given by $S(\pi,\pi)L^{2\beta_c/\nu} = f(\delta L^{1/\nu}, \beta/L^{z_c})$, where β_c is the critical exponent of the order parameter. Since the effective dimension is $d + z_c = 2 + 1 = 3$ and the broken symmetry is Z_2 symmetry, the quantum phase transition is expected to belong to the 3D Ising universality class. Thus, using the critical exponents $\nu = 0.63002$ and $2\beta_c/\nu = 1.03627$ of the 3D Ising universality class,[48] we plot g and $S(\pi,\pi)L^{2\beta_c/\nu}$ as functions of $\delta L^{1/\nu}$ with fixed β/L in Figs. 8(b) and 8(c), respectively. As shown in these figures, the data collapse for large systems agrees with the expected scaling behavior.

Separate determination of the SS-SF boundaries was carried out for low hopping amplitudes $zt/U \lesssim 0.08$ at $zV/U = 1$, because we observed clear finite jumps in the particle density. Figure 9 shows a jump at the SS-SF boundary, indicating a first-order transition. Similar discontinuities were also found in the previous quantum Monte Carlo study.[21] In this region, we determined the boundary from the position of the jump. The

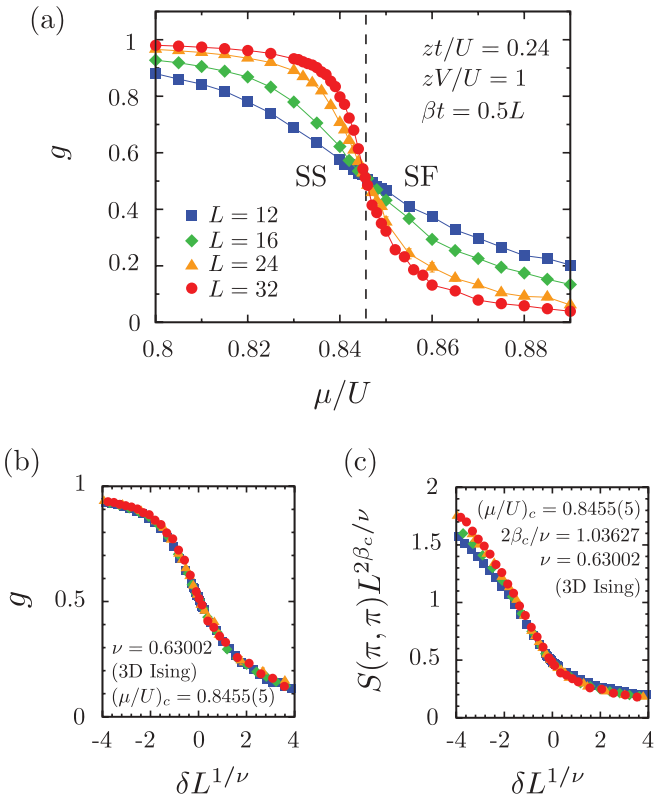

FIG. 8. (Color online) (a) Binder ratio g as a function of the chemical potential μ/U. The SS-SF boundary can be estimated from the crossing point of the curves for different system sizes. (b, c) Finite-size scaling plots of (b) g and (c) $S(\pi,\pi)L^{2\beta_c/\nu}$.

discontinuities of the SS-SF boundaries seem to be connected to those of the CB-MI boundaries in the classical limit $zt/U = 0$, where the particle density changes discontinuously from

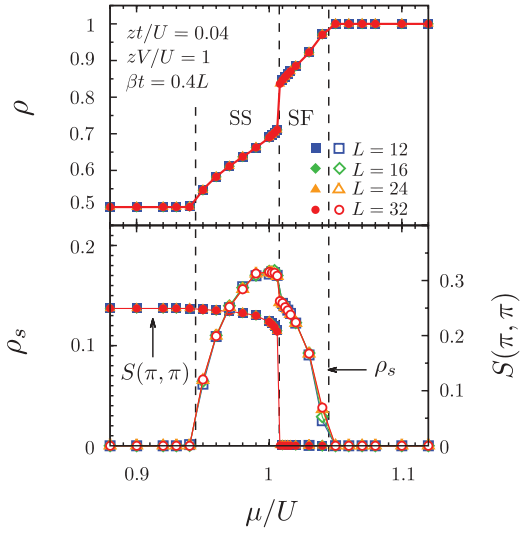

FIG. 9. (Color online) Particle density ρ, superfluid stiffness ρ_s, and structure factor $S(\pi,\pi)$ as functions of the chemical potential μ/U for a low hopping amplitude $zt/U = 0.04$. Finite jumps in the physical quantities can be observed at the SS-SF boundary. Dashed vertical lines are used to separate different phases. In the classical limit $zt/U = 0$, it is known that the particle density ρ changes discontinuously from 1/2 to 1 at $(\mu/U)_c = 1$.

1/2 to 1, 1 to 3/2, . . . at the critical points $(\mu/U)_c = 1,2,\ldots$, respectively. In fact, when the hopping amplitude decreases, the SS-SF transition points approach the classical critical points, as shown in Fig. 1(a), and we found that the finite jump becomes larger.

V. COMMENSURATE SUPERSOLID PHASE

Most SSs are realized by adding/removing particles to/from a commensurate insulating solid. When doped defects delocalize against phase separations and give rise to superfluidity in a solid, an SS state appears. In contrast to such an SS, the situation of an SS at commensurate filling factors is different, because no dopants are present. In this section, by obtaining simulation results in the canonical ensemble, we investigate the SS at the exact commensurate filling factor $\rho = 1/2$. To obtain results in the canonical ensemble by the grand-canonical method, we performed the following procedures. We first estimated the chemical potential that corresponds to the desired particle density with a high accuracy. Then we performed simulations at the obtained chemical potential and used only samples whose particle density is exactly equal to the desired value. Using this method, in Sec. V A, we obtain direct evidence for an SS at half-filling, excluding the possibility of phase separations. In Sec. V B, we present the ground-state phase diagram at half-filling. The obtained phase diagram shows that the SS phase becomes clearer as the nearest-neighbor repulsion zV/U increases, as suggested in the previous work based on the Gutzwiller approximation.[33]

A. Supersolid at half-filling

In this subsection, we explicitly show the presence of an SS at half-filling. In Fig. 10, we plot ρ_s and $S(\pi,\pi)$ as functions of the temperature at half-filling. At low temperatures, both ρ_s and $S(\pi,\pi)$ have finite values, indicating an SS state. To exclude the possibility of phase separations, we show a snapshot of the typical configuration in Fig. 11. In our snapshot, we do not find any macroscopic phase separations. Instead, we can see that the CB solid has microscopic defects (interstitials or vacancies), suggesting that the superfluidity is

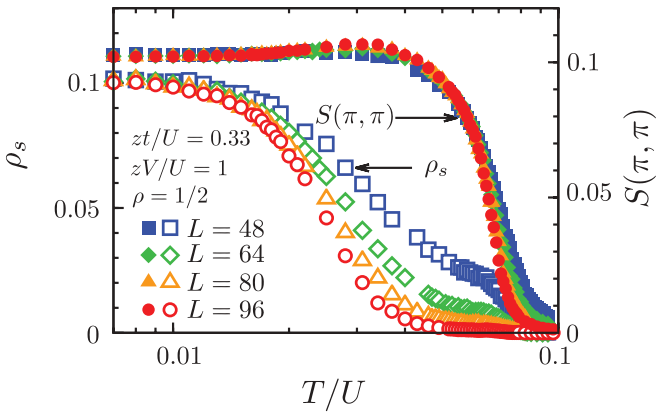

FIG. 10. (Color online) Finite-temperature dependence of the superfluid stiffness ρ_s and the structure factor $S(\pi,\pi)$ exactly at half-filling.

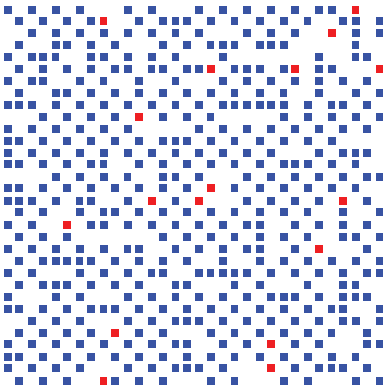

FIG. 11. (Color online) Snapshot of an SS at half-filling, showing a typical configuration in a real space at some particular imaginary time. The parameters are chosen at $(L,zt/U,zV/U,T/U) = (32,0.33,1,0.008)$. Each site is denoted as a square. Open, blue (dark gray), and red (light gray) squares indicate empty, singly occupied, and doubly occupied sites, respectively.

caused by the delocalization of defects in the same way as in the ordinary SSs. However, the origin of defects seems to be different from that in ordinary SS, because it is realized without any doping of particles or holes. Since the CB-SS transition at half-filling corresponds to the special transition at the tip of the CB lobe in the grand-canonical phase diagram, it is driven not by adding or subtracting a particle but by delocalizing quantum fluctuations. Therefore, it is reasonable to interpret the origin of defects as unbound interstitial-vacancy pairs due to the delocalizing quantum fluctuations.[5]

The melting of the SS occurs through two successive finite-temperature transitions, namely, SF and CB transitions. Each critical temperature can be determined as follows. We first consider the SF transition. In Fig. 10, we can observe the strong system size dependence of ρ_s above the SF region, which is characteristic of the Kosterlitz-Thouless transition.[49,50] To determine the critical temperature of the Kosterlitz-Thouless transition, we performed a χ^2 fit to the critical form for the mean-square winding number.[51,52] Specifically, the mean-square winding number follows the scaling form $(\pi/4)\langle W^2\rangle = 1 + [2\ln(L/L_0)]^{-1}$ at the critical point. Here, L_0 is the only free parameter. For each temperature, we performed a χ^2 fit to the critical form and measured χ^2. Finally, we obtain the critical temperature as the temperature that minimizes the value of χ^2. The result is shown in Fig. 12(a). From this analysis, we estimated the critical temperature of the Kosterlitz-Thouless transition as $(T/U)_c = 0.01700(25)$.

Next, we determined the critical temperature of the CB transition from the structure factor. For finite-temperature phase transitions, the scaling form is given by $S(\pi,\pi)L^{2\beta_c/\nu} = f(\delta L^{1/\nu})$, where $\delta = (T/U) - (T/U)_c$. Since the transition is related to Z_2 symmetry breaking, we expect that the critical exponents $2\beta_c/\nu$ and ν will equal 1/4 and 1, respectively, for the 2D Ising universality class. When this is the case, the curves of $S(\pi,\pi)L^{2\beta_c/\nu}$ for different system sizes should cross at the critical temperature. Figure 12(b) shows the result. In the inset, to check the consistency of the critical exponents, we present scaling plots that show excellent data collapse. Therefore, we obtained the critical temperature of the CB

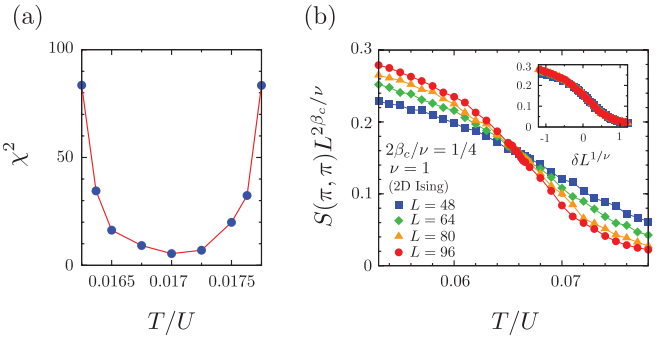

FIG. 12. (Color online) Determination of the two critical temperatures in the supersolid state. (a) Values of χ^2 [filled (blue) squares] for each temperature. At the critical temperature, the value of χ^2 is expected to be minimized. (b) $S(\pi,\pi)L^{2\beta_c/\nu}$ as a function of temperature. The intersection of the curves corresponds to the critical temperature of the checkerboard-solid transition. Inset: Data collapse of the scaling plots.

transition as $(T/U)_c = 0.066(1)$ from the intersection of the curves.

B. Ground-state phase diagram at half-filling

In the previous quantum Monte Carlo study,[21] an SS phase was not found at half-filling for $zt/U = 0.2$. According to the results obtained from the Gutzwiller approximation, this might be because the hopping amplitude was not sufficiently high for an SS to be clearly found at half-filling.[33] In this subsection, to confirm this hypothesis, we clarify the parameter dependence of the SS region at half-filling.

In Fig. 13, we present the ground-state phase diagram at half-filling in the zt/U-zV/U plane. The phase boundary is determined from the position of an intersection of g or $\rho_s L$ for different system sizes with the assumption that $z_c = 1$. Figure 14 shows the result at $zV/U = 1$. From this figure, we obtained the quantum critical points for the CB-SS and SS-SF transition as $(zt/U)_c = 0.32888(8)$ and $0.33332(8)$, respectively. Note that the critical point for the CB-SS

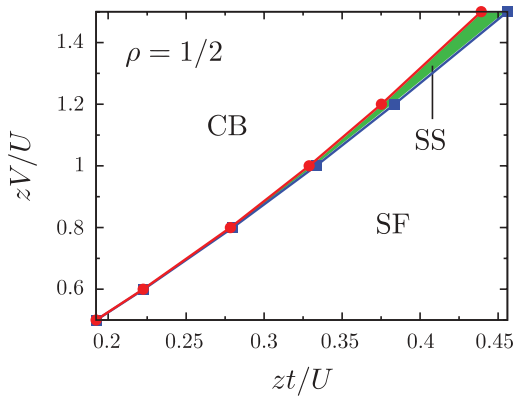

FIG. 13. (Color online) Ground-state phase diagram at half-filling. Circles and squares denote critical points corresponding to the onset of checkerboard order and superfluidity, respectively. Lines are guides for the eye. The shaded (green) region between the two lines represents the supersolid (SS) phase.

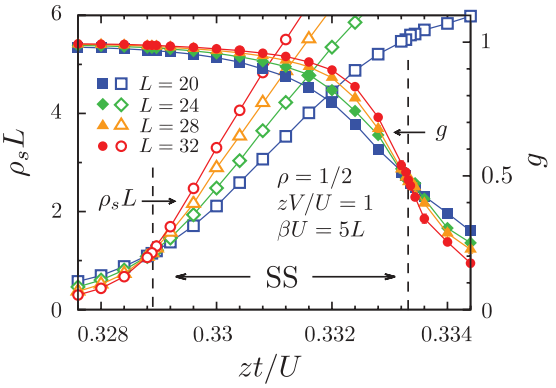

FIG. 14. (Color online) Scaled superfluid stiffness $\rho_s L$ and Binder ratio g as functions of hopping amplitude zt/U. Quantum critical points of the CB-SS and SS-SF transition can be estimated from the intersections of the curves of $\rho_s L$ and g, respectively. Dashed vertical lines are placed at the estimated quantum critical points for the CB-SS transition (left line) and the SS-SF transition (right line).

transition at $\rho = 1/2$ agrees with that obtained from the grand-canonical ensemble (Sec. IV B). In our phase diagram, the SS region is much smaller than that obtained by the Gutzwiller approximation.[33] However, the qualitative behaviors of the phase boundaries agree with the Gutzwiller results. As the nearest-neighbor repulsion zV/U increases, the CB phase expands up to higher hopping amplitudes zt/U. The SS phase also extends for large nearest-neighbor repulsions and hopping amplitudes. In contrast, for low hopping amplitudes including $zt/U = 0.2$, the two phase boundaries are very close to each other. Thus, we conclude that the reason the SS phase was not found at half-filling in the previous quantum Monte Carlo result[21] is that the hopping amplitude was too low for the SS phase to be observed clearly, as the author of Ref. 33 predicted.

VI. SUMMARY

We have investigated the ground-state phase diagrams of the 2D extended Bose-Hubbard model by performing unbiased quantum Monte Carlo simulations. In addition to the known SS phase above half-filling, we have found an SS phase below and at half-filling, in agreement with the previous result for 3D systems[26,30,32] and the Gutzwiller mean-field result.[33] However, we have also found that the SS regions clearly become smaller as the dimensionality decreases. In addition to these results, we have confirmed that in the case of a strong nearest-neighbor repulsion, the ground-state phase diagram becomes qualitatively different from that in the case of a weak nearest-neighbor repulsion. In particular, the SS region exists in a broad region up to high hopping amplitudes. As discussed in Ref. 34, this might lead to the experimental realization of an SS in the optical lattice systems. In such an SS region, we have observed the bimodal structure in the momentum distribution, which can be obtained by time-of-flight imaging. Since the bimodal structure exhibits the signatures of superfluidity and solidity simultaneously, we expect that this will provide clear evidence of the SS state.

ACKNOWLEDGMENTS

This work was financially supported by the Global COE Program "The Physical Science Frontier," a Grant-in-Aid for JSPS Fellows (No. 249904), a Grant-in-Aid for Scientific Research (B) (No. 22340111), and the Computational Materials Science Initiative (CMSI), Japan. The simulations were performed on computers at the Supercomputer Center, Institute for Solid State Physics, University of Tokyo.

*Corresponding author: ohgoe@issp.u-tokyo.ac.jp

[1] A. F. Andreev and I. M. Lifshitz, Sov. Phys. JETP **29**, 1107 (1969).
[2] G. V. Chester, Phys. Rev. A **2**, 256 (1970).
[3] E. Kim and M. H. W. Chan, Nature (London) **427**, 225 (2004).
[4] E. Kim and M. H. W. Chan, Science **305**, 1941 (2004).
[5] N. Prokof'ev and B. Svistunov, Phys. Rev. Lett. **94**, 155302 (2005).
[6] M. Boninsegni, A. B. Kuklov, L. Pollet, N. V. Prokof'ev, B. Svistunov, and M. Troyer, Phys. Rev. Lett. **97**, 080401 (2006).
[7] A. S. C. Rittner and J. D. Reppy, Phys. Rev. Lett. **97**, 165301 (2006).
[8] S. Sasaki, R. Ishiguro, F. Caupin, H. J. Maris, and S. Balibar, Science **313**, 1098 (2006).
[9] L. Pollet, M. Boninsegni, A. B. Kuklov, N. V. Prokof'ev, B. V. Svisunov, and M. Troyer, Phys. Rev. Lett. **98**, 135301 (2007).
[10] M. Boninsegni, A. B. Kuklov, L. Pollet, N. V. Prokof'ev, B. V. Svistunov, and M. Troyer, Phys. Rev. Lett. **99**, 035301 (2007).
[11] M. Greiner, O. Mandel, T. Esslinger, T. W. Hänsch, and I. Bloch, Nature **415**, 39 (2002).
[12] J. M. Sage, S. Sainis, T. Bergeman, and D. DeMille, Phys. Rev. Lett. **94**, 203001 (2005).
[13] K.-K. Ni, S. Ospelkaus, M. H. G. Miranda, A. Peer, B. Neyenhuis, J. J. Zirbel, S. Kotochigova, P. S. Julienne, D. S. Jin, and J. Ye, Science **322**, 231 (2008).
[14] S. Ospelkaus, A. Péer, J. J. Zirbel, B. Neyenhuis, S. Kotochigova, P. S. Julienne, J. Ye, and D. S. Jin, Nature Phys. **4**, 622 (2008).
[15] D. Jaksch, C. Bruder, J. I. Cirac, C. W. Gardiner, and P. Zoller, Phys. Rev. Lett. **81**, 3108 (1998).
[16] A. van Otterlo, K. H. Wagenblast, R. Blatin, C. Bruder, R. Fazio, and G. Schön, Phys. Rev. B **52**, 16176 (2005).
[17] G. G. Batrouni and R. T. Scalettar, Phys. Rev. Lett. **84**, 1599 (2000).
[18] K. Góral, L. Santos, and M. Lewenstein, Phys. Rev. Lett. **88**, 170406 (2002).
[19] S. Wessel and M. Troyer, Phys. Rev. Lett. **95**, 127205 (2005).
[20] M. Boninsegni and N. Prokof'ev, Phys. Rev. Lett. **95**, 237204 (2005).
[21] P. Sengupta, L. P. Pryadko, F. Alet, M. Troyer, and G. Schmid, Phys. Rev. Lett. **94**, 207202 (2005).
[22] G. G. Batrouni, F. Hébert, and R. T. Scalettar, Phys. Rev. Lett. **97**, 087209 (2006).
[23] S. Yi, T. Li, and C. P. Sun, Phys. Rev. Lett. **98**, 260405 (2007).
[24] T. Suzuki and N. Kawashima, Phys. Rev. B **75**, 180502(R) (2007).
[25] L. Dang, M. Boninsegni, and L. Pollet, Phys. Rev. B **78**, 132512 (2008).
[26] K. Yamamoto, S. Todo, and S. Miyashita, Phys. Rev. B **79**, 094503 (2009).
[27] I. Danshita and C. A. R. Sá de Melo, Phys. Rev. Lett. **103**, 225301 (2009).
[28] L. Pollet, J. D. Picon, H. P. Büchler, and M. Troyer, Phys. Rev. Lett. **104**, 125302 (2010).
[29] B. Capogrosso-Sansone, C. Trefzger, M. Lewenstein, P. Zoller, and G. Pupillo, Phys. Rev. Lett. **104**, 125301 (2010).
[30] B. Xi, F. Ye, W. Chen, F. Zhang, and G. Su, Phys. Rev. B **84**, 054512 (2011).
[31] D. Yamamoto, I. Danshita, and C. A. R. Sá de Melo, Phys. Rev. A **85**, 021601(R) (2012).
[32] T. Ohgoe, T. Suzuki, and N. Kawashima, Phys. Rev. Lett. **108**, 185302 (2012).
[33] T. Kimura, Phys. Rev. A **84**, 063630 (2011).
[34] M. Iskin, Phys. Rev. A **83**, 051606(R) (2011).
[35] A. Griesmaier, J. Werner, S. Hensler, J. Stuhler, and T. Pfau, Phys. Rev. Lett. **94**, 160401 (2005).
[36] N. V. Prokof'ev, B. V. Svistunov, and I. S. Tupitsyn, Sov. Phys. JETP **87**, 310 (1998).
[37] O. F. Syljuåsen and A. W. Sandvik, Phys. Rev. E **66**, 046701 (2002).
[38] N. Kawashima and K. Harada, J. Phys. Soc. Jpn. **73**, 1379 (2004).
[39] Y. Kato and N. Kawashima, Phys. Rev. E **79**, 021104 (2009).
[40] E. L. Pollock and D. M. Ceperley, Phys. Rev. B **36**, 8343 (1987).
[41] D. L. Kovrizhin, G. V. Pai, and S. Shinha, Europhys. Lett. **72** (2005).
[42] T. Ohgoe, T. Suzuki, and N. Kawashima, J. Phys. Soc. Jpn. **80**, 113001 (2011).
[43] M. P. A. Fisher, P. B. Weichman, G. Grinstein, and D. S. Fisher, Phys. Rev. B **40**, 546 (1989).
[44] Y. Kato and N. Kawashima, Phys. Rev. E **81**, 011123 (2010).
[45] B. Capogrosso-Sansone, N. V. Prokof'ev, and B. V. Svistunov, Phys. Rev. B **75**, 134302 (2007).
[46] B. Capogrosso-Sansone, S. G. Söyler, N. Prokof'ev, and B. Svistunov, Phys. Rev. A **77**, 015602 (2008).
[47] M. Campostrini, M. Hasenbusch, A. Pelissetto, P. Rossi, and E. Vicari, Phys. Rev. B **63**, 214503 (2001).
[48] M. Hasenbusch, Phys. Rev. B **82**, 174433 (2010).
[49] J. M. Kosterlitz and D. J. Thouless, J. Phys. C **6**, 1181 (1973).
[50] J. M. Kosterlitz, J. Phys. C **7**, 1046 (1974).
[51] H. Weber and P. Minnhagen, Phys. Rev. B **37**, 5986 (1988).
[52] K. Harada and N. Kawashima, J. Phys. Soc. Jpn. **67**, 2768 (1998).